Journal of Materials Chemistry A

ROYAL SOCIETY OF CHEMISTRY

PAPER

View Article Online
View Journal | View Issue

Cite this: J. Mater. Chem. A, 2026, 14, 10745

Revealing the pseudocapacitance charge storage mechanism of sulfur-doped carbon supercapacitors in non-aqueous electrolyte through *in situ* EPR

Tobias Neff,†[ab] Friedrich Stemmler,†[c] Leonhard Kolb,[b] Joris van Slageren [c] and Anke Krueger *[a]

Sulfur-doped carbon has emerged as a promising material for high-performance supercapacitors, yet its charge storage mechanism in non-aqueous electrolytes remains poorly understood. In this study, we provide an experimentally supported mechanism, that the pseudocapacitive behaviour of S-doped carbon is governed by a reversible polaron-to-bipolaron transition, facilitated by thiophenic sulfur sites. *In situ* electron paramagnetic resonance (EPR) spectroscopy is consistent with the presence of pre-existing polarons, which undergo oxidation to bipolarons during charging and revert to polarons during discharge, establishing a clear correlation between spin chemistry and charge storage. Electrochemical characterization, including cyclic voltammetry, Trasatti, and Dunn analysis, reveals that up to 81% of the total capacitance originates from faradaic contributions, which is due to the presence of sulfur-doped carbon. Comparison with mesoporous onion-like carbon (OLC), whose capacitance arises from a purely electric double-layer (EDL), further supports this conclusion. These findings provide the first description of a proposed pseudocapacitive charge storage mechanism in sulfur-doped carbon within organic electrolytes, that is supported by comprehensive experiments. This result lays the foundation for future optimized sulfur-doped electrode materials.

Received 19th September 2025
Accepted 24th January 2026

DOI: 10.1039/d5ta07697h

rsc.li/materials-a

1 Introduction

The transition to the use of renewable energy requires advanced storage technologies to ensure grid stability and efficient energy management.[1] Supercapacitors have emerged as a critical component in this transition, offering rapid charge–discharge capability, high power density and exceptional cycling stability.[2] Unlike batteries, supercapacitors store energy by electrochemical double layer formation, avoiding bulk chemical reactions. This provides a unique lifetime of up to more than 100 000 cycles,[3] but limits the energy density.[4] Since the stored energy scales with the square of the operating voltage ($E \propto U^2$), achieving higher voltages is essential to maximise energy density.[5] Organic electrolytes, such as $TEABF_4$ (tetraethylammonium tetrafluoroborate) in acetonitrile, allow higher voltages than aqueous systems which are limited by the water splitting potential.[6,7] However, the larger ions in organic electrolytes have a lower charge density and interact less strongly with the electrode surfaces than the small, hydrated ions in aqueous systems. As a result, organic electrolytes possess lower specific capacitances and hence lower energy densities.[6,8,9] To further increase energy density, the integration of pseudocapacitive materials into supercapacitors, capable of storing charge through reversible faradaic reactions, has gained significant interest.[10,11] By enabling fast, reversible faradaic reactions, pseudocapacitive materials offer improved energy storage without compromising the power density and cycling stability of supercapacitors.[12] In aqueous systems, pseudocapacitive materials such as transition metal oxides like RuO_2,[13] MnO_2 (ref. 14 and 15) and conductive polymers[16,17] have shown exceptional performance due to proton exchange reactions. However, the transfer of pseudocapacitive mechanisms to organic systems has proved more challenging due to the stringent requirements for chemical stability, redox reversibility and compatibility with organic electrolytes.

Conductive polymers, such as poly(3,4-ethylenedioxythiophene) (PEDOT), exhibit excellent conductivity and redox activity in aqueous[18] and organic electrolytes,[19] enabling their use in high performance supercapacitors. Similarly, heteroatom doping of carbon materials, particularly with nitrogen (N),[20,21] sulfur (S)[22] or phosphorus (P),[23] has been shown to modify and often improve the electronic properties and introduce active sites for faradaic reactions even in aprotic

[a]Institute of Organic Chemistry, University of Stuttgart, Pfaffenwaldring 55, Stuttgart, 70569, Germany. E-mail: anke.krueger@oc.uni-stuttgart.de
[b]Institute for Organic Chemistry, Julius-Maximilian University Würzburg, Am Hubland, 97074 Würzburg, Germany
[c]Institute of Physical Chemistry, University of Stuttgart, Pfaffenwaldring 55, 70569 Stuttgart, Germany
† Equal contribution.

organic electrolytes, where proton transfer reactions are not possible. Sulfur doping introduces structural and electronic modifications in carbon materials, potentially enabling polaron-mediated faradaic reactions.[24] Due to this, sulfur-doped carbons offer a promising alternative to conducting polymers such as PEDOT, which often suffer from poor rate capability.[19] While in aqueous media the storage mechanisms of hetero-doped carbons are well understood and widely studied,[25,26] the pseudocapacitive mechanisms of sulfur-doped carbons in non-aqueous environments remain largely unexplored.[27] This lack of knowledge limits the rational design and optimization of sulfur-doped materials for supercapacitors, making further investigation essential.

Inspired by PEDOT, we propose a model in which sulfur doping in carbons facilitates the formation of bipolarons on the positive electrode during charging as the primary mechanism for faradaic charge storage. Like in PEDOT, the sulfur-doped sites enable the reversible formation of polarons and bipolarons, which seem to be responsible for the pseudocapacitive behaviour. To validate this hypothesis, we used *in situ* electron paramagnetic resonance spectroscopy, which is well suited to probe the dynamics of polarons and bipolarons. EPR revealed clear evidence of bipolaron formation during electrochemical cycling, suggesting that the charge storage mechanism on the positive electrode is radical-based. This is in contrast to previous studies that propose negative polarization of the sulfur atom by the cation without experimental evidence.[22,27] This experimental study provides the first evidence for a theoretical framework that proposes reversible transition to an EPR-silent oxidized state, consistent with polaron to bipolaron formation, for pseudocapacitive charge storage in sulfur-doped carbons in organic electrolytes.

2 Material and methods

The synthesis of the active material was performed as already reported in our previous publication.[28] For convenience, the procedures and analytical data are provided here again.

2.1 Synthesis of active material[28]

Polythiophene was synthesized and subsequently utilized as a precursor material for the synthesis of sulfur-doped carbon. The sample underwent thermal annealing under vacuum conditions (~0.5 mbar) in a tube furnace (STF 16/450, Carbolite Gero GmbH, Germany). The temperature was regulated using an integrated digital temperature controller (3216 P1, Eurotherm). A heating rate of 5 K min^{-1} was applied until the target temperature of 700 °C was reached, which was then maintained for a duration of 3 hours. Onion-like carbon was produced by annealing purified detonation nanodiamond powder (Gansu Lingyun Corp., China) at 1500 °C for 2 hours vacuum conditions (~0.5 mbar) with the same heating rate.

2.2 Structural characterization[28]

The Raman spectrum of sulfur-doped carbon was recorded using a DXR Raman Microscope (Thermo Fisher Scientific, USA) with a 532 nm excitation wavelength. The measurements were conducted at a laser power of 0.2 mW, with 50 repetitions and an exposure time of 20 seconds per acquisition. X-ray photoelectron spectroscopy (XPS) measurements were carried out on an uncycled electrode. The analysis was performed using an unmonochromatized Al Kα X-ray source, coupled with a Sienta R3000 analyzer. The acquired spectra were fitted with pseudo-Voigt profiles and corrected using a Shirley-type background.

2.3 Electron microscopy

High-resolution transmission electron microscopy (HRTEM) was performed by dispersing the carbon powders in isopropanol *via* ultrasonication and depositing the dispersion onto a lacey carbon-coated copper grid (Plano GmbH, Germany). The analysis was conducted using an FEI Titan 80–300 microscope (Thermo Fisher Scientific, USA) at an operating voltage of 300 kV.

2.4 Electrode preparation

For the electrode preparation of sulfur-doped carbon and the mixture with 20% OLC, a slurry was prepared using carboxymethyl cellulose (CMC) as binder (degree of substitution: 1.2; molar mass: 250 kg mol^{-1}, Acros organics) and deionized water as solvent. All components were mixed together in the mass ratio 50 : 10 : 1 for distilled water : active material : binder and vigorously stirred for 48 h using a magnetic stirrer. For the OLC slurry, the same preparation parameters were used, but beforehand OLC was preagglomerated according to a procedure described in a previous work[29] in order to be able to use the same binder content. All slurries were doctor bladed onto carbon coated Aluminium foil (Zflo 2653, Transcontinental Advanced Coatings, USA), resulting in an average mass loading of ~2 mg cm^{-2}. The electrodes were dried in a drying oven at 130 °C at ambient pressure for several hours. For electrochemical analysis, they were subsequently die cut with a punching iron and pressed with a hydraulic press (*ca.* 0.2 GPa) yielding round electrodes (14 mm diameter).

2.5 Electrochemical characterization

To conduct the electrochemical characterization of the electrodes, symmetrical cells were assembled using a stainless-steel test cell (ECC-Ref, El-Cell, Germany), separated by a Celgard 2325 (PP/PE/PP) separator with a thickness of 0.025 mm (Polypore, USA). The electrolyte was prepared as a 1 M solution of tetraethylammonium tetrafluoroborate ($TEABF_4$; TCI, Germany) in anhydrous acetonitrile (Sigma Aldrich, USA). In the absence of humidity (<1 ppm) and oxygen (<1 ppm), three test cells were assembled for each material using a glovebox (N_2, Labmaster 130, M. Braun Inertgas-Systeme, Germany). Cyclic voltammetry (CV) was performed using a potentio-/galvanostat VMP300 (Bio-Logic instruments, France) within the voltage range of 0–2.5 V.

2.6 EPR spectroscopy

For *in situ* measurements, an in-house developed two electrode setup in a symmetrical full cell configuration was assembled.

The cell consisted of two platinum wires, which were both coated with the active material, inserted into a standard X-band EPR tube. The electrochemical cell was prepared under nitrogen atmosphere utilizing oxygen-free anhydrous acetonitrile and 1 M solution of tetraethylammonium tetra-fluoroborate ($TEABF_4$; TCI, Germany) as electrolyte. Directly after preparation, the electrochemical cell was left to equilibrate overnight and cycled at least twice at a scan rate of 1 mV s^{-1} over the entire voltage range of 0 V to 2.5 V prior to measurement. For the measurement, the EPR tube was partially inserted into the microwave resonator such that only the working electrode (WE) was located inside the resonator. In this way, exclusively EPR-active species resulting from processes at the WE were monitored. Voltage dependent *in situ* measurements were conducted at constant applied electrode potentials with a step size of 100 mV per spectrum. EPR measurements were started once the current reached values close to zero. For more in depth *in situ* measurements, the cell was cycled continuously at 1 mV s^{-1} with EPR spectra recorded every 42 seconds. Voltage dependent contributions from OLC or CMC binder were ruled out (Fig. S1).

The measurements were conducted on a Bruker EMX X-band EPR spectrometer at room temperature with X-band irradiation. The spectra were fitted with the EasySpin (Version 6.0.0-dev.53) software package for Matlab (Version R2022a) using a spin Hamiltonian with an isotropic g tensor and Lorentzian line-broadening factors.

3 Results and discussion

3.1 Structural characterization

The synthesized sulfur-doped carbon material exhibits a sulfur content of 30.4% relative to carbon, as determined by elemental analysis. The material used in this study originates from the same synthesis batch as that used in our previous publication on the fabrication of highly efficient and stable sodium-ion batteries. The elemental analysis data reported previously are referenced here.[28] This significant level of sulfur incorporation, which exceeds that of typical surface adsorption, suggests that sulfur atoms are embedded into the carbon framework in various bonding configurations. A schematic representation of a possible structure, showing sulfur integrated as thiophenic and oxidized functional groups, is provided in Fig. 1.

Raman spectroscopic analysis (Fig. 1A) was employed to reveal the structural key characteristics of the material. A broad C–S band was observed between 200 and 500 cm^{-1}, indicating the formation of sulfur-carbon bonds.[30] The broad D-band at 1350 cm^{-1} is associated with disordered and partially amorphous carbon[31] and the G-band at 1566 cm^{-1} corresponds to graphitic carbon.[32] The intensity ratio $I_D/I_G = 0.88$ indicates a substantial degree of structural disorder and the presence of defects, which can be introduced by functional groups or the significant presence of amorphous carbon.[33] To complement the Raman results, transmission electron microscopy was used to examine the material's morphology. The TEM images (Fig. 1B) show that the carbon structure is predominantly disordered, with regions of short-range ordering. X-ray photoelectron spectroscopy analysis provides a detailed chemical fingerprint of sulfur species present in the material. The S2p spectrum (Fig. S2) reveals two primary peaks: the dominant species at 164.0 eV, corresponding to thiophenic sulfur covalently bonded within the carbon framework, and another at 169.2 eV, attributed to oxidized sulfur species. The thiophenic sulfur thus confirms the successful incorporation of sulfur into the carbon matrix, while the oxidized sulfur species suggest surface functionalization. A more detailed deconvolution of the XPS analysis of this batch of material, can be found in a previous work of our group, in which the sodium-ion storage

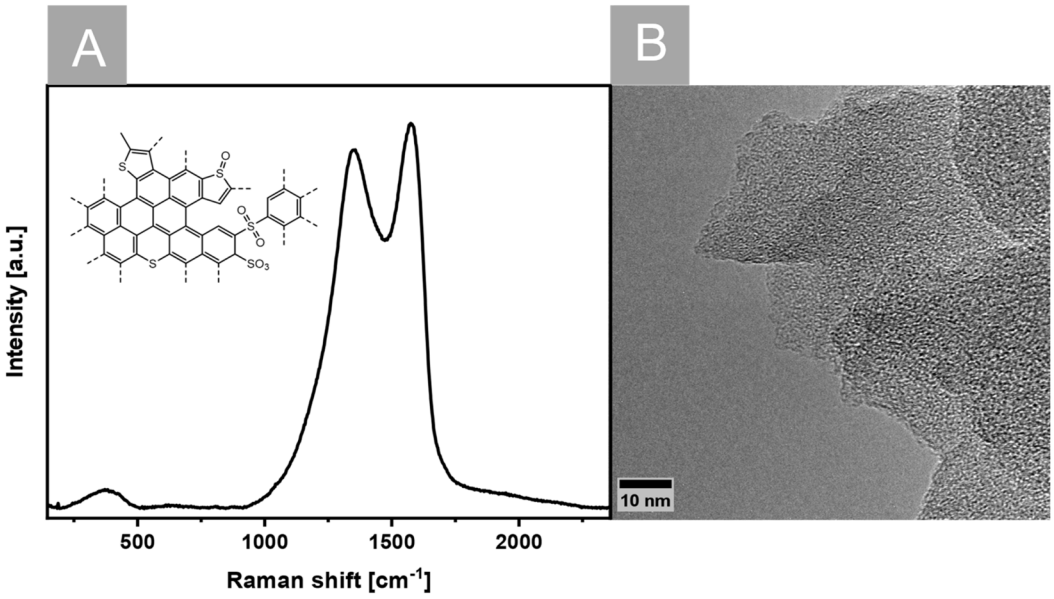

Fig. 1 Schematic representation of the structure of sulfur-doped carbon and its characterization by (A) Raman spectrum, including the C–S bond; (B) TEM image revealing a disordered structure. For more detailed characterization of the material refer to ref. 28.

capabilities were explored.[28] These data are being reused here for consistency.

3.2 Electrochemical characterization

The electrochemical performance of the sulfur-doped carbon material was evaluated using full-cell supercapacitors. Initial cyclic voltammetry measurements of the pure material at a scan rate of 2.5 mV s^{-1} (Fig. S3) revealed curves that deviate significantly from the rectangular profile typical of electric double-layer capacitance, and display prominent redox peaks. Furthermore, the material exhibited suboptimal performance at increased scan rates, indicating limitations in its intrinsic conductivity and charge transfer kinetics. To address these limitations, further electrochemical tests were conducted using electrodes composed of the sulfur-doped material blended with 20% onion-like carbon. OLC, with its high electrical conductivity and mesoporous structure, was selected as a suitable additive. OLC's nearly exclusive EDL contribution ensures that its presence does not interfere with the material's inherent pseudocapacitive properties (Fig. S4). The addition of OLC resulted in significantly improved CV profiles, allowing for improved qualitative and quantitative evaluations.

As demonstrated in Fig. 2A, the CV curves of the electrodes manifest a quasi-rectangular shape, accompanied by discernible redox peaks observed at a cathodic potential of 1.2 V and an anodic potential of 1.1 V. These peaks indicate a reversible redox reaction, thereby substantiating the pseudocapacitive nature of the charge storage mechanism inherent in the sulfur-doped material.[34] The strong redox signals in S-doped carbon, and their absence in OLC indicate the active participation of sulfur functionalities in the charge–discharge process. The specific capacitance of the device (C_m) and an individual electrode (C_E) was determined by performing measurements in a two-electrode full cell configuration at different scan rates (ν) within a voltage window (ΔV) of 2.5 V. The values were normalized to the combined mass (m) of the deposited materials on both electrodes and calculated according to the following equations:

$$C_m = \frac{\int_{V_0}^{V_1} I(V)\mathrm{d}V}{2\ \nu\ \times m \times \Delta V} \quad (1)$$

$$C_E = 4C_m \quad (2)$$

The dependence of capacitance on the scan rate (Fig. 2B) provides further evidence of pseudocapacitive behaviour, with a steep decline in capacitance observed up to 10 mV s^{-1}, beyond which the rate of decline diminishes noticeably. This behaviour is indicative of the kinetic limitations of redox reactions at higher scan rates, thereby further substantiating the role of pseudocapacitance (PS) in the charge storage process.

The electrochemical behaviour of the sulfur-doped carbon material was further analysed using Trasatti and Dunn methodologies to elucidate the contributions of faradaic and non-faradaic processes.[35–37] Trasatti analysis was employed to distinguish between pseudocapacitive and electric double-layer capacitance mechanisms. The Trasatti analysis was performed by plotting the specific capacitance C as a function of the inverse square root of the scan rate ($\nu^{-1/2}$).[38] The extrapolated values, as illustrated in Fig. 3A, provide a clear quantification of the charge storage mechanisms. The total capacitance C_T at $\nu \rightarrow 0$ represents the maximum achievable capacitance from both faradaic and EDL processes. Conversely, the capacitance at $\nu \rightarrow \infty$ corresponds to the EDL contribution, which is directly proportional to the scan rate and reflects purely non-faradaic charge storage (Fig. 3B). The faradaic contribution was determined to be 83% of the total capacitance by calculating the difference between these two extrapolated values. This significant fraction suggests a dominant role of pseudocapacitive redox reactions introduced by sulfur groups, such as thiophenic and oxidized sulfur, within the material.

Dunn's method was used to further analyse the charge storage contributions at different scan rates, providing insight into the rate-dependent behaviour of the material.[39] The CV responses (Fig. 3C) and subsequent analysis at further scan

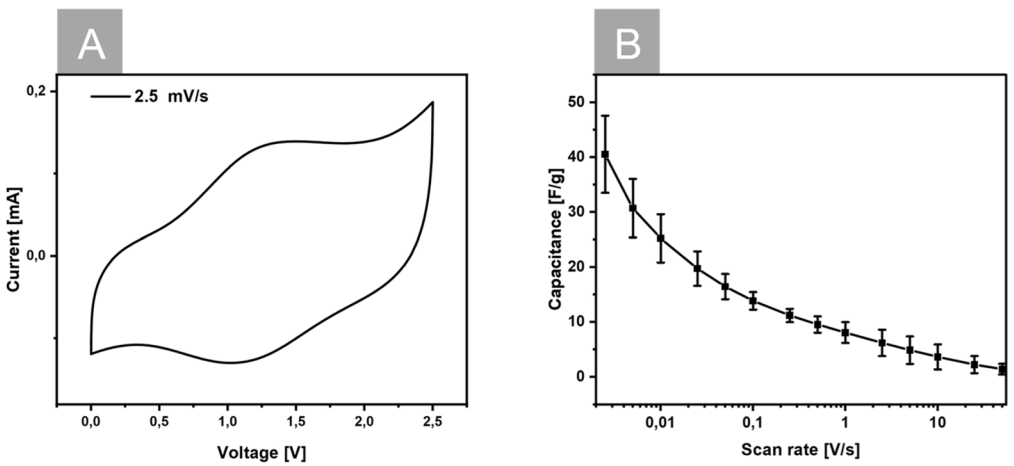

Fig. 2 Electrochemical performance of sulfur-doped carbon with 20% OLC: (A) cyclic voltammogram at 2.5 mV s^{-1}, showing prominent redox peaks; (B) capacitance as a function of scan rate. The line is a guide to the eye.

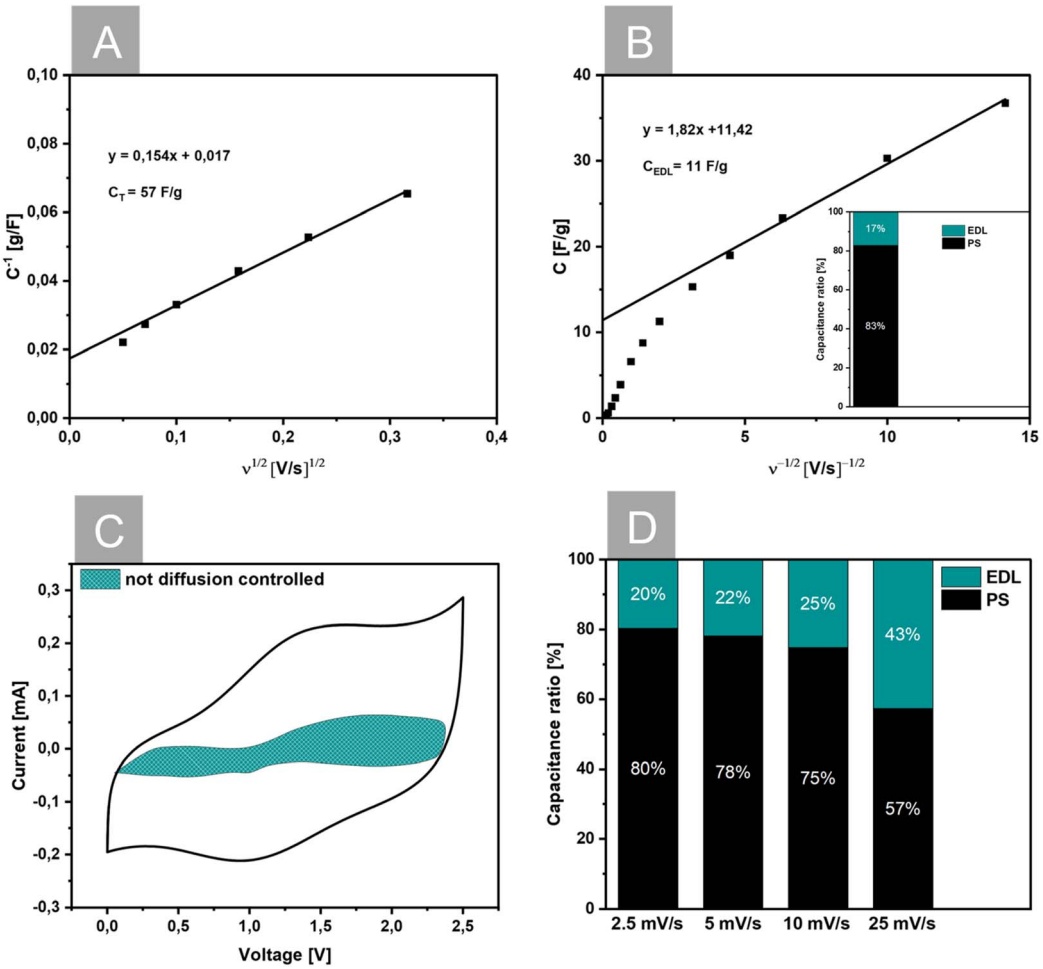

Fig. 3 Electrochemical analysis of sulfur-doped carbon using Trasatti and Dunn methods. Trasatti plot showing (A) the extrapolated total capacitance and (B) EDL proportion with an insert showing the ratio of pseudocapacitive (PS) and EDL fractions. (C) Diffusion independent contribution to charge storage at a scan rate of 2.5 mV s^{-1}. (D) Relative contribution ratio of EDL and PS charge storage at different scan rates.

rates revealed pseudocapacitive contributions of 80%, 78%, 75% and 57% at 2.5, 5.0, 10 and 25 mV s^{-1} respectively. The high pseudocapacitive fraction at low scan rates underscores the efficiency of the sulfur redox sites, while the decreasing contribution at higher rates highlights the kinetic limitations associated with redox processes. These results are consistent with observations from the Trasatti analysis and emphasize the role of sulfur functionalities as the primary contributors to the pseudocapacitive behaviour of the material.

Overall, the electrochemical analysis shows that sulfur-doped carbon exhibits a significant pseudocapacitance driven by reversible redox reactions at sulfur sites. While these results highlight the potential of the material, the precise mechanism underlying this redox activity remains elusive. To date, no comprehensive model or experimental data has been identified to conclusively explain this behaviour for sulfur-doped carbon in organic electrolytes. Hypotheses from related hetero-doped carbon materials, such as nitrogen-doped reduced graphene oxide, suggest that radicals may play a role in the observed phenomena.[40] It is also known that thiophene sulfur-containing polymers, such as PEDOT, accumulate polaron and bi-polaron radical species during oxidation.[41] In addition, the electrolyte properties of $TEABF_4$ in acetonitrile are particularly favourable for a polaronic charge storage mechanism. In acetonitrile, the moderate solvation of both TEA^+ and BF_4^- and the reduced tendency for strong ion pairing increase the availability of mobile counter-ions at the electrode interface.[6] Furthermore BF_4^- is a weakly coordinating anion with a highly delocalized negative charge, which in return favours the stabilization of delocalized positive charge within the electrode material. The investigation of this possibility requires advanced techniques capable of probing interactions at the molecular level.

In this context, *in situ* electron resonance spectroscopy is a powerful analytical tool. By monitoring changes in the EPR spectra due to oxidative processes at the working electrode in a symmetrical cell configuration. EPR provides direct insight into the redox processes occurring during charge and discharge of a single electrode, excluding processes on the counter electrode. This separation of electrode processes was implemented by only placing the working electrode inside the resonator. This allows for the avoidance of overlapping effects from processes of the counter electrode, which is an issue of pure

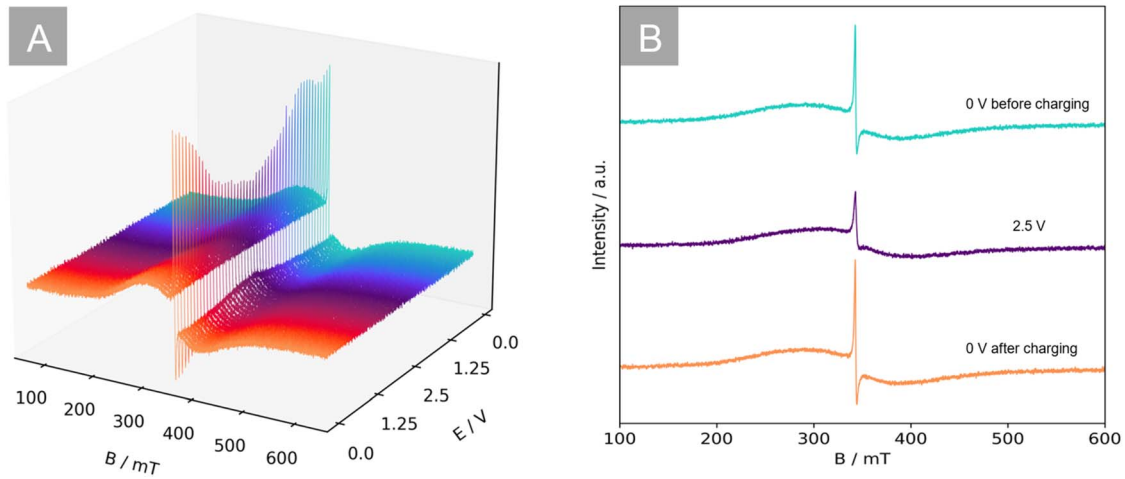

Fig. 4 (A) *In situ* EPR spectra acquired at different voltages during charging and discharging of the material. (B) Selection of EPR spectra at three different voltages during the charging and discharging process, highlighting the reversible change in signal intensity of the sharp spectral feature.

electrochemical testing of full cells.[42] The spectra obtained from these experiments, shown in Fig. 4, reveal critical details about the involvement of radicals and the nature of the underlying mechanism.

At 0 V, the EPR spectrum shows two distinct components: a broad signal centred around $g \approx 2$ and a sharp feature at $g = 2.0023(2)$, corresponding to the g-value of a free electron.[43] This is similar to the paramagnetic species observed immediately after synthesis (Fig. S5). Both components exhibit asymmetric characteristics, indicative of a Dysonian line shape, which is commonly observed in conducting materials with dimensions larger than the microwave skin depth, such as conductive carbon materials.[44,45] In the discharged state, the sharp signal is more asymmetric than the broad signal. During charging, the Dysonian character of this resonance line becomes more pronounced. The typical derivative feature of the EPR signal changes to a predominantly absorption-like shape at 2.5 V. The narrow linewidth of 1.6(1) mT at 0 V increases upon charging, while the signal intensity decreases as the applied voltage increases. Upon discharge, the sharp feature returns reversibly to its initial state. Inspecting the broad signal, it undergoes a slight reduction in intensity upon charging to 2.5 V, while the asymmetry increases slightly during this process. The peak-to-peak linewidth of 90(10) mT remains relatively constant across the whole voltage window. Upon discharge of the cell, the signal intensity recovers and returns to the level of the uncharged state. The increased linewidth and small voltage dependence attributes this signal to a paramagnetic metal-containing impurity, possibly embedded during synthesis, as is well known from literature.[40]

The sharp signal in the discharged state is more asymmetric than the broad signal. To further analyse the results, a more detailed *in situ* EPR spectrum of the sharp signal at $g = 2.0023$

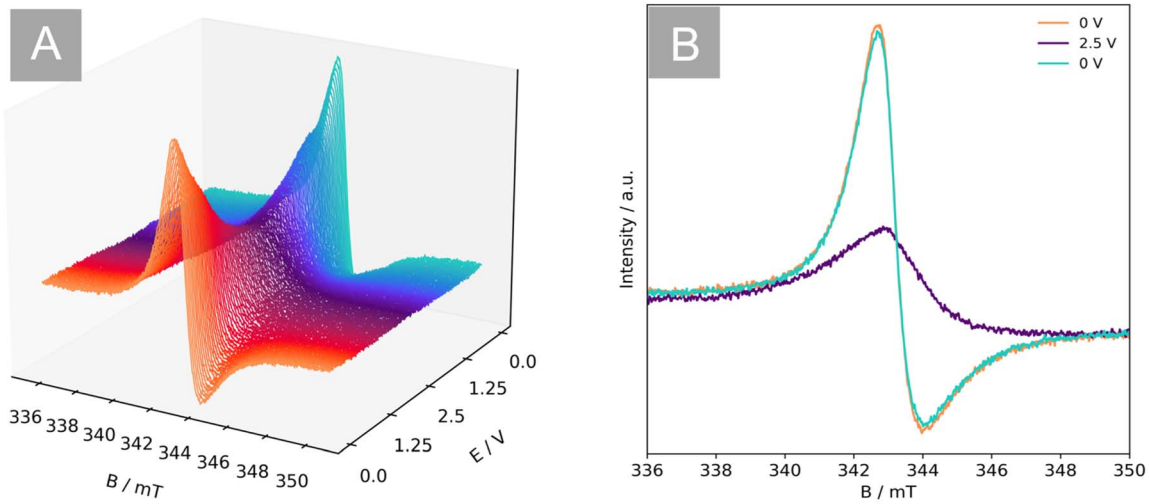

Fig. 5 (A) *In situ* EPR scan of the $g \approx 2$ field region, with the signal evolution clearly visible. (B) EPR scans at voltages of 0 V (uncharged, orange), 2.5 V (charged, purple) and 0 V (discharged, cyan). The signal recovers completely to the uncharged state prior measurement.

was continuously measured during charging/discharging with 1 mV s^{-1}, shown in Fig. 5.

The $g \approx 2$ region shows the same signal intensity evolution during both charging and discharging as in Fig. 4. A closer inspection reveals that the signal comprises two distinct components at 0 V applied: one Dysonian line, which is independent of voltage, and one voltage-dependent Lorentzian line with a *g*-value of 2.0023. Despite the high resolution of the spectrum, the strong Dysonian lineshape of the sharp signal makes it difficult to apply double integration to determine signal intensity as a function of voltage. Under assumption that the Lorentzian EPR signal intensity reaches zero in the fully charged state, the spectrum at 2.5 V consists only of the Dysonian component. Subtracting the Dysonian spectrum acquired at 2.5 V from all the other spectra results in the leftover signal, which can be fitted as a Lorentzian line (Fig. S7). Considering only the corrected spectra, a clearer evolution of the Lorentzian signal during charging (Fig. 6A) and discharging (Fig. 6B) is obtained. Double integration of the resulting data reveals the change in intensity of the Lorentzian line during both charging and discharging, as shown in Fig. 6C. The signal intensity evolves linearly with the applied voltage after an initial onset at 0 V, with the discharge process showing the opposite behaviour.

The reversible voltage-dependent change in signal intensity suggests a behaviour comparable with a polaron-like species. The material used here is composed of building blocks, which contain thiophene like sulfur, similar to the conductive polymer PEDOT, which is known to exhibit polarons and their reversible polaron-to-bipolaron oxidation.[46,47] The *g*-values of the paramagnetic polaron species are comparable to those measured in the sulfur-containing conductive polymers presented here.[41,48] The change of signal intensity during charge and discharge processes correlate with the proposed polaron-to-bipolaron-to-polaron transition in conductive polymers.[49] Upon charging, these pre-existing polarons undergo oxidation to form bipolarons, which are EPR inactive, decreasing the signal intensity. Those bipolarons are reversibly reduced during discharge, recovering the initial polaron EPR signal. It is important to note that *in situ* EPR directly probes the population of localized $S = 1/2$ states, while the oxidized end state itself is EPR silent. Consequently, the disappearance of the EPR signal reflects a transition to a spin-silent oxidized state but does not by itself

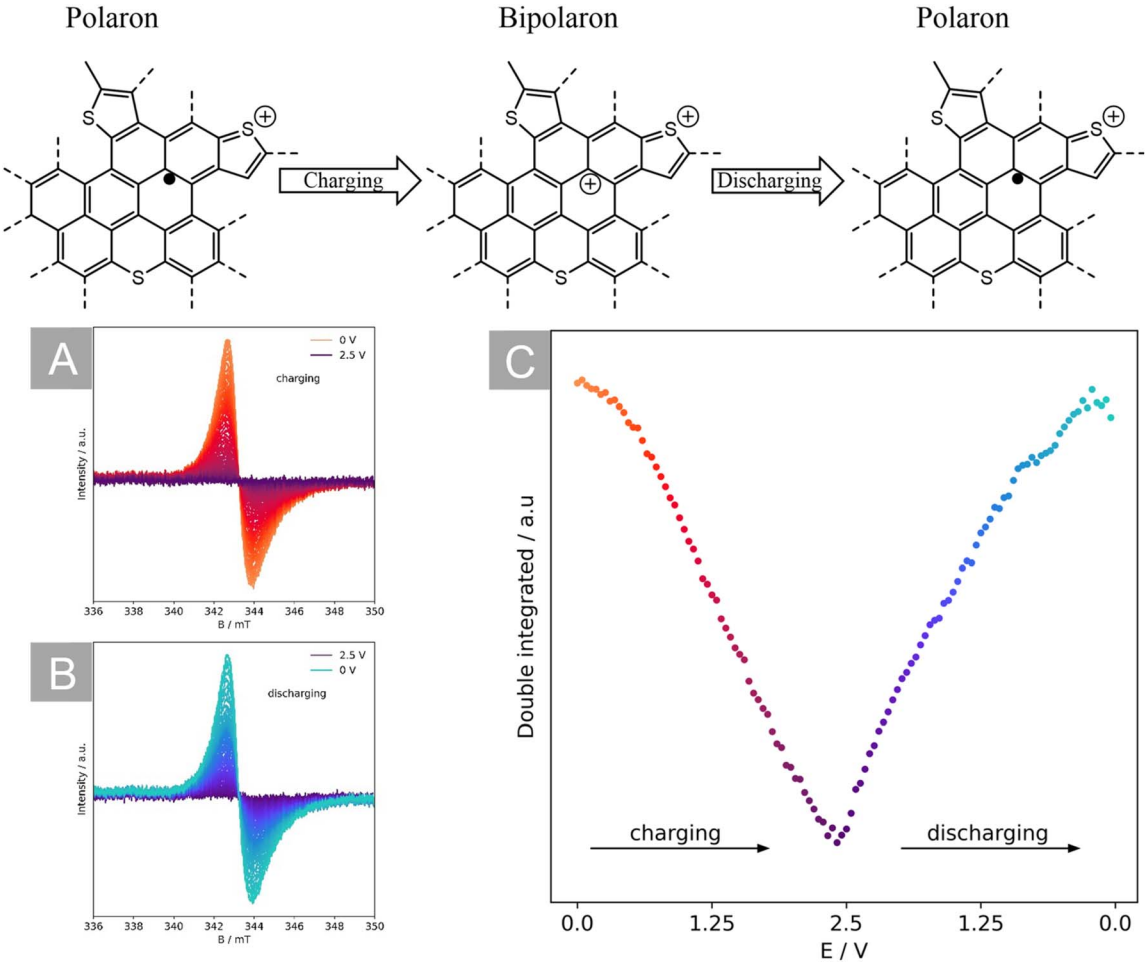

Fig. 6 (A) EPR spectra acquired during charging after subtraction of the signal at 2.5 V (B) EPR spectra acquired during discharging after subtraction of the signal at 2.5 V (C) voltage dependent double integral of the Lorentzian line at $g = 2.0023$ with a scheme of the model of polaron state changes.

allow an unambiguous distinction between different EPR silent configurations. Therefore, the formation of localized, EPR-silent ionic states at isolated defect or edge sites cannot be fully excluded. However, such a mechanism is unlikely to dominate under positive electrode polarization and in the presence of weakly coordinating BF_4^- anions, as it would not account for the high, fast, and fully reversible pseudocapacitive contribution observed over a large fraction of the accessible surface.

Consequently, the proposed mechanism of a bipolaron formation, analogous to cathodic conductive polymers, explains both the observed decrease in signal intensity and the reversible intensity evolution during the charge/discharge cycle, as well as the recovery of the signal after discharge. The possible presence of such polarons could explain the pseudocapacitive behaviour of the material. The polaron charge carriers, being localized at the sulfur containing thiophene units, are further oxidized during the charging process, and are stabilized through the electrolyte counterion BF_4^-.

Although it is possible that some of the polarons present are not oxidised in the fully charged state, it is difficult to distinguish these species within the dysonian line at 2.5 V without introducing undue complexity. However, a clear decrease in signal intensity is observed during charging, even without applying complex data analysis.

The combined spectroelectrochemical and electrochemical data strongly support the hypothesis that the pseudocapacitive behaviour of sulfur-doped carbon is driven by the presence of polarons, which are oxidized to bipolarons during charging. Notably, this reversible spin modulation was not observed in onion-like carbon, a reference material, which shows a lack pseudocapacitive behaviour in non-aqueous electrolytes in reference measurements (Fig. S4 and S5). This distinction is further reinforced by Trasatti analysis, which reveals a negligible faradaic contribution for onion-like carbon, in stark contrast to the significant pseudocapacitive fraction observed in sulfur-doped carbon. These findings highlight the critical role of sulfur atoms in facilitating the polaronic mechanism. To the best of our knowledge, this represents the first experimental evidence elucidating the pseudocapacitive behaviour of sulfur-doped carbon and its underlying redox mechanism.

4 Conclusion

This study provides mechanistic insights to the charge storage mechanism of sulfur-doped carbon supercapacitors in organic electrolyte environment. The investigated material exhibits an unexpected high pseudocapacitive contribution of 81% regarding its charge storage. We propose that this behaviour can be explained by a reversible polaron-to-bipolaron transition facilitated by sulfur atoms within the carbon framework. The presence of polarons in sulfur-doped carbon has been experimentally evidenced and described in the context of supercapacitors, supported by electrochemical *in situ* EPR measurements. These findings suggest that polarons, induced by thiophenic sulfur, are directly responsible for the observed pseudocapacitive charge storage.

To the best of our knowledge, this study provides the first experimental supported description of the pseudocapacitive behaviour of sulfur-doped carbon and its associated redox mechanism in non-aqueous environment. The proposed mechanism highlights the essential role of sulfur atoms in facilitating reversible redox activity and sheds light on the unique electrochemical properties of the material. These findings lay a basis for the rational design and optimization of other sulfur-doped carbons, enabling their development for high performance supercapacitor applications.

Conflicts of interest

The authors declare no conflict of interest.

Data availability

Data for this article, including ESR data, electrochemical data, Raman spectroscopy data and TEM data are available upon publication at DaRUS repository at https://doi.org/10.18419/DARUS-5358.

Supplementary information (SI) is available. See DOI: https://doi.org/10.1039/d5ta07697h.

Acknowledgements

The financial support of this project by the Bavarian State Ministry of the Environment and Consumer Protection (TNT01NaT-72356 "Umweltverträgliche Anwendungen der Nanotechnologie weiterentwickeln: Na + NanoBatterie") and the State of Baden-Wurttemberg is gratefully acknowledged. We acknowledge financial support by the Deutsche Forschungsgemeinschaft DFG (German Research Foundation, project ID 358283783 – SFB 1333/2 2022). We thank the Fraunhofer Institute for Silicate Research for access to the potentio-/galvanostat and Mara Göttlinger and Vilija Anfimovaite for the introduction to the operation of the setup. We acknowledge Florian Kaufmann for the measurement of the transmission electron micrographs and thank Johannes Heßdörfer and Friedrich Reinert for the XPS measurements as reported in (ref. 28). During the preparation of this work, the authors used DeepL write in order to improve English spelling, fluency and language polishing. After using this tool, the authors reviewed and edited the content as needed and take full responsibility for the content of the publication.

References

1 Z. Yang, J. Zhang, M. C. W. Kintner-Meyer, X. Lu, D. Choi, J. P. Lemmon and J. Liu, Electrochemical Energy Storage for Green Grid, *Chem. Rev.*, 2011, **111**(5), 3577–3613.
2 A. Burke, Ultracapacitors: why, how, and where is the technology, *J. Power Sources*, 2000, **91**(1), 37–50.
3 M. Czagany, S. Hompoth, A. K. Keshri, N. Pandit, I. Galambos, Z. Gacsi and P. Baumli, Supercapacitors: An Efficient Way for Energy Storage Application, *Materials*, 2024, **17**(3), 702.

4 Y. Zhu, S. Murali, M. D. Stoller, K. J. Ganesh, W. Cai, P. J. Ferreira, A. Pirkle, R. M. Wallace, K. A. Cychosz, M. Thommes, D. Su, E. A. Stach and R. S. Ruoff, Carbon-Based Supercapacitors Produced by Activation of Graphene, *Science*, 2011, **332**(6037), 1537–1541.
5 Y. Gogotsi and P. Simon, True Performance Metrics in Electrochemical Energy Storage, *Science*, 2011, **334**(6058), 917–918.
6 A. Acharjee and B. Saha, Organic electrolytes in electrochemical supercapacitors: Applications and developments, *J. Mol. Liq.*, 2024, **400**, 124487.
7 P. Simon and Y. Gogotsi, Materials for electrochemical capacitors, *Nat. Mater.*, 2008, **7**(11), 845–854.
8 V. Barranco, M. A. Lillo-Rodenas, A. Linares-Solano, A. Oya, F. Pico, J. Ibañez, F. Agullo-Rueda, J. M. Amarilla and J. M. Rojo, Amorphous Carbon Nanofibers and Their Activated Carbon Nanofibers as Supercapacitor Electrodes, *J. Phys. Chem. C*, 2010, **114**(22), 10302–10307.
9 J. K. McDonough, A. I. Frolov, V. Presser, J. Niu, C. H. Miller, T. Ubieto, M. V. Fedorov and Y. Gogotsi, Influence of the structure of carbon onions on their electrochemical performance in supercapacitor electrodes, *Carbon*, 2012, **50**(9), 3298–3309.
10 D. Potphode and C. S. Sharma, Pseudocapacitance induced candle soot derived carbon for high energy density electrochemical supercapacitors: Non-aqueous approach, *J. Energy Storage*, 2020, **27**, 101114.
11 D. Hulicova, M. Kodama and H. Hatori, Electrochemical Performance of Nitrogen-Enriched Carbons in Aqueous and Non-Aqueous Supercapacitors, *Chem. Mater.*, 2006, **18**(9), 2318–2326.
12 O. Boujibar, A. Ghosh, O. Achak, T. Chafik and F. Ghamouss, A high energy storage supercapacitor based on nanoporous activated carbon electrode made from Argan shells with excellent ion transport in aqueous and non-aqueous electrolytes, *J. Energy Storage*, 2019, **26**, 100958.
13 P. Wang, Y. Xu, H. Liu, Y. Chen, J. Yang and Q. Tan, Carbon/carbon nanotube-supported RuO2 nanoparticles with a hollow interior as excellent electrode materials for supercapacitors, *Nano Energy*, 2015, **15**, 116–124.
14 W. Guo, C. Yu, S. Li, Z. Wang, J. Yu, H. Huang and J. Qiu, Strategies and insights towards the intrinsic capacitive properties of MnO2 for supercapacitors: Challenges and perspectives, *Nano Energy*, 2019, **57**, 459–472.
15 S. Yao, S. Wang, R. Liu, X. Liu, Z. Fu, D. Wang, H. Hao, Z. Yang and Y.-M. Yan, Delocalizing the d-electrons spin states of Mn site in MnO2 for anion-intercalation energy storage, *Nano Energy*, 2022, **99**, 107391.
16 N. Kurra, M. K. Hota and H. N. Alshareef, Conducting polymer micro-supercapacitors for flexible energy storage and Ac line-filtering, *Nano Energy*, 2015, **13**, 500–508.
17 A. Eftekhari, L. Li and Y. Yang, Polyaniline supercapacitors, *J. Power Sources*, 2017, **347**, 86–107.
18 M. E. Plonska-Brzezinska, M. Lewandowski, M. Błaszyk, A. Molina-Ontoria, T. Luciński and L. Echegoyen, Preparation and Characterization of Carbon Nano-Onion/PEDOT:PSS Composites, *ChemPhysChem*, 2012, **13**(18), 4134–4141.
19 C. Bauer, M. Kirchner and A. Krueger, In situ polymerization of EDOT onto sulfonated onion-like carbon for efficient pseudocapacitor electrodes, *Energy Adv.*, 2024, **3**(6), 1422–1430.
20 S.-M. Li, S.-Y. Yang, Y.-S. Wang, H.-P. Tsai, H.-W. Tien, S.-T. Hsiao, W.-H. Liao, C.-L. Chang, C.-C. M. Ma and C.-C. Hu, N-doped structures and surface functional groups of reduced graphene oxide and their effect on the electrochemical performance of supercapacitor with organic electrolyte, *J. Power Sources*, 2015, **278**, 218–229.
21 D. He, J. Niu, M. Dou, J. Ji, Y. Huang and F. Wang, Nitrogen and oxygen co-doped carbon networks with a mesopore-dominant hierarchical porosity for high energy and power density supercapacitors, *Electrochim. Acta*, 2017, **238**, 310–318.
22 S. Shaheen Shah, S. M. Abu Nayem, N. Sultana, A. J. Saleh Ahammad and M. Abdul Aziz, Preparation of Sulfur-doped Carbon for Supercapacitor Applications: A Review, *ChemSusChem*, 2022, **15**(1), e202101282.
23 G. Lin, Q. Wang, X. Yang, Z. Cai, Y. Xiong and B. Huang, Preparation of phosphorus-doped porous carbon for high performance supercapacitors by one-step carbonization, *RSC Adv.*, 2020, **10**(30), 17768–17776.
24 L. Niu, T. Wu, D. Zhou, J. Qi and Z. Xiao, Polaron hopping-mediated dynamic interactive sites boost sulfur chemistry for flexible lithium-sulfur batteries, *Energy Storage Mater.*, 2022, **45**, 840–850.
25 J.-S. M. Lee, M. E. Briggs, C.-C. Hu and A. I. Cooper, Controlling electric double-layer capacitance and pseudocapacitance in heteroatom-doped carbons derived from hypercrosslinked microporous polymers, *Nano Energy*, 2018, **46**, 277–289.
26 A. Gopalakrishnan and S. Badhulika, Effect of self-doped heteroatoms on the performance of biomass-derived carbon for supercapacitor applications, *J. Power Sources*, 2020, **480**, 228830.
27 Y. Huang, S. L. Candelaria, Y. Li, Z. Li, J. Tian, L. Zhang and G. Cao, Sulfurized activated carbon for high energy density supercapacitors, *J. Power Sources*, 2014, **252**, 90–97.
28 T. Neff, J. Heßdörfer, A. Bilican, L. Kolb, F. Reinert and A. Krueger, Superior Sulfur-Doped Carbon Anodes for Sodium-Ion Batteries through Incorporation of Onion-Like Carbon, *Electrochim. Acta*, 2025, 146912.
29 C. Bauer, A. Bilican, S. Braxmeier, G. Reichenauer and A. Krueger, Sustainable supercapacitor electrodes based on preagglomerated carbon onions and a green binder, *Carbon*, 2022, **197**, 555–562.
30 X.-g. Yu, J.-y. Xie, J. Yang, H.-j. Huang, K. Wang and Z.-s. Wen, Lithium storage in conductive sulfur-containing polymers, *J. Electroanal. Chem.*, 2004, **573**(1), 121–128.
31 A. C. Ferrari and J. Robertson, Interpretation of Raman spectra of disordered and amorphous carbon, *Phys. Rev. B:Condens. Matter Mater. Phys.*, 2000, **61**(20), 14095–14107.
32 D. Roy, M. Chhowalla, H. Wang, N. Sano, I. Alexandrou, T. W. Clyne and G. A. J. Amaratunga, Characterisation of

carbon nano-onions using Raman spectroscopy, *Chem. Phys. Lett.*, 2003, **373**(1), 52–56.
33 P. Zhang, J. Fan, Y. Wang, Y. Dang, S. Heumann and Y. Ding, Insights into the role of defects on the Raman spectroscopy of carbon nanotube and biomass-derived carbon, *Carbon*, 2024, **222**, 118998.
34 Y. Zhou, R. Ma, S. L. Candelaria, J. Wang, Q. Liu, E. Uchaker, P. Li, Y. Chen and G. Cao, Phosphorus/sulfur Co-doped porous carbon with enhanced specific capacitance for supercapacitor and improved catalytic activity for oxygen reduction reaction, *J. Power Sources*, 2016, **314**, 39–48.
35 R. Raavi, S. Archana, P. Adinarayana Reddy and P. Elumalai, Performances of dual carbon multi-ion supercapacitors in aqueous and non-aqueous electrolytes, *Energy Adv.*, 2023, **2**(3), 385–397.
36 M. Isacfranklin, R. Yuvakkumar, G. Ravi, D. Velauthapillai, M. Pannipara and A. G. Al-Sehemi, Superior supercapacitive performance of Cu2MnSnS4 asymmetric devices, *Nanoscale Adv.*, 2021, **3**(2), 486–498.
37 T. Schoetz, L. W. Gordon, S. Ivanov, A. Bund, D. Mandler and R. J. Messinger, Disentangling faradaic, pseudocapacitive, and capacitive charge storage: A tutorial for the characterization of batteries, supercapacitors, and hybrid systems, *Electrochim. Acta*, 2022, **412**, 140072.
38 S. Ardizzone, G. Fregonara and S. Trasatti, "Inner" and "outer" active surface of RuO2 electrodes, *Electrochim. Acta*, 1990, **35**(1), 263–267.
39 J. Wang, J. Polleux, J. Lim and B. Dunn, Pseudocapacitive Contributions to Electrochemical Energy Storage in TiO2 (Anatase) Nanoparticles, *J. Phys. Chem. C*, 2007, **111**, 14925–14931.
40 B. Wang, V. Likodimos, A. J. Fielding and R. A. W. Dryfe, In situ Electron paramagnetic resonance spectroelectrochemical study of graphene-based supercapacitors: Comparison between chemically reduced graphene oxide and nitrogen-doped reduced graphene oxide, *Carbon*, 2020, **160**, 236–246.
41 A. Zykwinska, W. Domagala, A. Czardybon, B. Pilawa and M. Lapkowski, In situ EPR spectroelectrochemical studies of paramagnetic centres in poly(3,4-ethylenedioxythiophene) (PEDOT) and poly(3,4-butylenedioxythiophene) (PBuDOT) films, *Chem. Phys.*, 2003, **292**(1), 31–45.
42 M. Sathiya, J. B. Leriche, E. Salager, D. Gourier, J. M. Tarascon and H. Vezin, Electron paramagnetic resonance imaging for real-time monitoring of Li-ion batteries, *Nat. Commun.*, 2015, **6**(1), 6276.
43 J. R. Harbour and M. J. Walzak, Effect of electroreduction on the EPR spectra due to charge carriers in carbon blacks, *Carbon*, 1985, **23**(6), 687–690.
44 F. J. Dyson, Electron Spin Resonance Absorption in Metals. II. Theory of Electron Diffusion and the Skin Effect, *Phys. Rev.*, 1955, **98**(2), 349–359.
45 G. Feher and A. F. Kip, Electron Spin Resonance Absorption in Metals. I. Experimental, *Phys. Rev.*, 1955, **98**(2), 337–348.
46 I. Zozoulenko, A. Singh, S. K. Singh, V. Gueskine, X. Crispin and M. Berggren, Polarons, Bipolarons, And Absorption Spectroscopy of PEDOT, *ACS Appl. Polym. Mater.*, 2019, **1**(1), 83–94.
47 O. Bubnova, Z. U. Khan, H. Wang, S. Braun, D. R. Evans, M. Fabretto, P. Hojati-Talemi, D. Dagnelund, J.-B. Arlin, Y. H. Geerts, S. Desbief, D. W. Breiby, J. W. Andreasen, R. Lazzaroni, W. M. Chen, I. Zozoulenko, M. Fahlman, P. J. Murphy, M. Berggren and X. Crispin, Semi-metallic polymers, *Nat. Mater.*, 2014, **13**(2), 190–194.
48 W. Domagala, B. Pilawa and M. Lapkowski, Quantitative in-situ EPR spectroelectrochemical studies of doping processes in poly(3,4-alkylenedioxythiophene)s: Part 1: PEDOT, *Electrochim. Acta*, 2008, **53**(13), 4580–4590.
49 C. Nicolaides, E. Nicolaidou, P. Papagiorgis, G. Itskos, S. C. Hayes and T. Trypiniotis, Effect of structural conformation of conjugated polymers on spin transport, *Phys. Rev. Mater.*, 2022, **6**(9), 095601.